version 1.0
March 27, 2013

Studies of the photoproduction of isolated photons with and without a jet at HERA.

ZEUS Collaboration

Abstract

Isolated-photon production in photoproduction, both inclusive and together with a jet, has been measured with the ZEUS detector at HERA using an integrated luminosity of $370\,\text{pb}^{-1}$. Differential cross sections are presented in the isolated-photon transverse-energy and pseudorapidity ranges $6 < E_T^{\gamma} < 15\,\text{GeV}$ and $-0.7 < \eta^{\gamma} < 0.9$, and for jet transverse-energy and pseudorapidity ranges $4 < E_T^{\text{jet}} < 35\,\text{GeV}$ and $-1.5 < \eta^{\text{jet}} < 1.8$, for exchanged photon virtualities $Q^2 < 1\,\text{GeV}^2$. Differential cross sections are also presented for inclusive isolated photon production as functions of the transverse momentum and pseudorapidity of the photon. Higher-order theoretical calculations are compared to the results.

1 Introduction

Events in which an isolated high-energy photon is observed can provide a direct probe of the underlying partonic process in high-energy collisions involving hadrons, since the emission of such photons is largely unaffected by parton hadronisation. Processes of this kind have been studied in a number of fixed-target and hadron-collider experiments [1]. In *ep* collisions at HERA, the ZEUS and H1 collaborations have previously reported the production of isolated photons in photoproduction [2–7], in which the exchanged photon is quasi-real, and also in deep inelastic scattering (DIS) [8–11]. In this paper, earlier photoproduction measulurements by ZEUS are extended to make use of the full HERA II data set. The statistical precision is much improved owing to the availability of much higher integrated luminosity. Measurements are presented of isolated photon production at high transverse energy with and without an accompanying jet requirement.

Figure 1 gives examples of the lowest-order (LO) diagrams for high-energy photon photoproduction in quantum chromodynamics (QCD). In "direct" production processes, the entire incoming photon is absorbed by a quark from the incoming proton, while in "resolved" processes, the photon's hadronic structure provides a quark or gluon that interacts with a parton from the proton. Processes in which the photon is radiated at the perturbative QCD level are commonly called "prompt"[1]. Another class of processes, in which a photon is produced in association with a jet, also illustrated in Fig. 1, are referred to as "fragmentation" processes. Photons radiated from the incoming and outgoing electron give rise to an observed scattered electron in the detector, and such events are ignored in this measurement.

Perturbative QCD predictions are compared to the measurements. The cross sections for isolated photon production in photoproduction have been calculated to order $O(\alpha^3\alpha_s)$ by M. Fontannaz *et al.* (FGH) [12,13]. A calculation based on the k_T factorisation approach has been made by Baranov *et al.* (BLZ) [14].

2 Experimental set-up

The measurements are based on a data sample corresponding to an integrated luminosity of $370 \pm 1\,\mathrm{pb}^{-1}$, taken during the years 2004 to 2007 with the ZEUS detector at HERA. During this period, HERA ran with an electron/positron beam energy of 27.5 GeV and a proton beam energy of 920 GeV. The sample is a sum of e^+p and e^-p data[2].

[1] An alternative commonly-used nomenclature is to refer to "prompt" photons as "direct"; thus Figs. 1a,c would be called "direct-direct" and "resolved-direct" diagrams, respectively.

[2] Hereafter "electron" refers to both electrons and positrons unless otherwise stated.

A detailed description of the ZEUS detector can be found elsewhere [15]. Charged particles were tracked in the central tracking detector (CTD) [16] and a silicon micro vertex detector (MVD) [17] which operated in a magnetic field of 1.43 T provided by a thin superconducting solenoid. The high-resolution uranium–scintillator calorimeter (CAL) [18] consisted of three parts: the forward (FCAL), the barrel (BCAL) and the rear (RCAL) calorimeters. The BCAL covered the pseudorapidity range –0.74 to 1.01 as seen from the nominal interaction point. The FCAL and RCAL extended the range to –3.5 to 4.0. The smallest subdivision of the CAL is referred to as a cell. The barrel electromagnetic calorimeter (BEMC) cells had a pointing geometry aimed at the nominal interaction point, with a cross section approximately $5 \times 20\,\mathrm{cm}^2$, with the finer granularity in the Z-direction[3]. This fine granularity allows the use of shower-shape distributions to distinguish isolated photons from the products of neutral meson decays such as $\pi^0 \to \gamma\gamma$.

The luminosity was measured using the Bethe–Heitler reaction $ep \to e\gamma p$ by a luminosity detector which consisted of two independent systems: a lead–scintillator calorimeter [19] and a magnetic spectrometer [20].

3 Event selection and reconstruction

A three-level trigger system was used to select events online [15, 21, 22] by requiring well isolated electromagnetic deposits in the CAL. The trigger efficiency was approximately flat above a photon transverse energy of 4.5 GeV and had an absolute uncertainty in its value of 5%. Events were initially selected offline by requiring a high-energy photon candidate of transverse energy $> 3.5\,\mathrm{GeV}$ recorded in the ZEUS BCAL. To reduce background from non-ep collisions, events were required to have a reconstructed vertex position, Z_{vtx}, within the range $|Z_{\mathrm{vtx}}| < 40\,\mathrm{cm}$. No scattered beam electron was permitted, and photoproduction events were selected by the requirement $0.2 < y_{JB} < 0.7$, where $y_{JB} = \sum_i E_i(1 - \cos\theta_i)/2E_e$ and E_e is the energy of the electron beam. Here, E_i is the energy of the i-th CAL cell, θ_i is its polar angle and the sum runs over all cells [23].

Energy-flow objects (EFOs) [24] were constructed from calorimeter-cell clusters, associated with tracks when appropriate. Photon candidates were identified as trackless EFOs for which at least 90% of the reconstructed energy was measured in the BEMC. EFOs with wider electromagnetic showers than are typical for a single photon were accepted to allow

[3] The ZEUS coordinate system is a right-handed Cartesian system, with the Z axis pointing in the proton beam direction, referred to as the "forward direction", and the X axis pointing left towards the center of HERA. The coordinate origin is at the nominal interaction point. The pseudorapidity is defined as $\eta = -\ln\left(\tan\frac{\theta}{2}\right)$, where the polar angle, θ, is measured with respect to the proton beam direction.

evaluation of backgrounds. The reconstructed transverse energy of the photon candidate, E_T^γ, was required to lie within the range $6 < E_T^\gamma < 15$ GeV and the pseudorapidity, η^γ, had to satisfy $-0.7 < \eta^\gamma < 0.9$. The upper limit on the reconstructed transverse energy was selected to ensure that the shower shapes from the hadronic background and the photon signal remained distinguishable.

Each event was required to contain a photon candidate. Jet reconstruction was performed on all EFOs in the event, including the electron and photon candidates, using the k_T clustering algorithm [25] in the E-scheme in the longitudinally invariant inclusive mode [26] with the R parameter set to 1.0. The jets were required to have transverse energy, $E_T^{\rm jet}$, between 4 and 35 GeV and to lie within the pseudorapidity, $\eta^{\rm jet}$, range $-1.5 < \eta^{\rm jet} < 1.8$. One of the jets found by this procedure corresponds to or includes the photon candidate. An additional accompanying jet was required; if more than one was found, that with the highest $E_T^{\rm jet}$ was used.

To reduce both the background from photons and neutral mesons within jets and the fragmentation contribution, the photon candidate was required to be isolated from the reconstructed tracks and other hadronic activity. Photons radiated from beam leptons are also suppressed by requiring no observed scattered lepton in the apparatus. The isolation from tracks was achieved by demanding $\Delta R > 0.2$, where $\Delta R = \sqrt{(\Delta\phi)^2 + (\Delta\eta)^2}$ is the distance to the nearest reconstructed track with momentum greater than 250 MeV in the $\eta - \phi$ plane, where ϕ is the azimuthal angle. This selection was applied only at the detector level, and not in hadron or parton level calculations. Isolation from other hadronic activity was imposed by requiring that the photon candidate possessed at least 90% of the total energy of the reconstructed jet of which it formed a part.

The sample at this stage was dominated by background events. The largest source of background came from events in which one or more neutral mesons such as π^0 and η, decaying to photons, produced a photon candidate in the BEMC.

4 Theory

The LO QCD processes relevant here are the direct and resolved photoproduction processes (Fig. 1), in which there is a coupling to the incoming and outgoing photon and a single QCD vertex. Higher-order processes include the next-to-leading-order diagrams and fragmentation processes, in which a photon is produced within an outgoing jet. A box diagram term also contributes significantly at next-to-next-to-leading order.

Two theoretical predictions are compared to the measurements presented in this paper. In the approach of FGH [12,13], the LO and NLO diagrams and the box diagram term are calculated explicitly. Fragmentation processes are calculated in terms of a fragmentation function in which a quark or gluon gives rise to photon. Theoretical uncertainties arise due to the choice of factorisation and fragmentation scales, and were estimated by varying these scales by factors of 0.5 and 2.0. The k_T factorisation method used by BLZ [14] makes use of unintegrated parton densitities in the proton, and gives a quark-radiated contribution that is enhanced relative to the leading-order collinear approximations. Fragmentation and box terms, which contribute around 20% to the FGH calculation, are not included. Other uncertainties of up to 20% in the BLZ calculation are due mainly to the procedure of selecting jets from the evolution cascade in the factorisation approach.

In evaluating the predictions for the present data, both calculations have incorporated the experimental selections and photon-isolation procedure at the parton level. Hadronisation corrections were evaluated (see Section 5) to enable the predictions to be compared to the experimental data which are corrected to the hadron level.

5 Monte Carlo event simulation

Monte Carlo event samples were generated to evaluate the detector acceptance and to provide signal and background distributions. The program Pythia 6.416 [28] was used to simulate isolated photon emission for the study of the event-reconstruction efficiency. Pythia generates the direct and resolved processes at LO, next-to-leading-order (NLO) processes where a hard outgoing quark radiates a photon, and processes in which a fragmentation photon is radiated within a jet. The exchanged photon was required to have a virtuality of less than 1 GeV^2. As a check and to enable systematic uncertainties to be estimated, event samples were also generated using the Herwig program.

The generated MC events were passed through the ZEUS detector and trigger simulation programs based on Geant 3.21 [34]. They were reconstructed and analysed by the same programs as the data.

Backgrounds to the isolated photons arise from decays of neutral mesons in hadronic jets, in which the fragmentation by chance produces an energy cluster in the BCAL that passes the selection criteria for a photon. Samples of dijet events were generated using Pythia to enable background events to be extracted and used in the analysis. Events in which a high-energy photon was produced in either an NLO or a fragmentation process, as modelled by the MC, were excluded from the background sample.

Hadronisation corrections to the theory calculations were evaluated using Pythia and Herwig, and typically lowered the theoretical prediction by about 5% with typical uncertainties of a few percent. They were calculated by running the same jet algorithm and event selections on the generated partons and on the hadronised final state in the MC events, apart from the removal of charged tracks close to the photon.

6 Extraction of the photon signal

The event sample selected according to the criteria described in Section 3 was dominated by background; thus the photon signal was extracted statistically following the approach used in previous ZEUS analyses [2–4, 10, 11].

The photon signal was extracted from the background using the width, measured in the Z-direction, of the BEMC energy-cluster comprising the photon candidate. This was calculated as the variable $\langle \delta Z \rangle = \sum_i E_i |Z_i - Z_{\rm cluster}| \; / (w_{\rm cell} \sum_i E_i)$. Here, Z_i is the Z position of the centre of the i-th cell, $Z_{\rm cluster}$ is the centroid of the EFO cluster, $w_{\rm cell}$ is the width of the cell in the Z direction, and E_i is the energy recorded in the cell. The sum runs over all BEMC cells in the EFO.

The global distribution of $\langle \delta Z \rangle$ in the data and in the MC are shown in Fig. 2 for inclusive photon events and those containing a jet. The $\langle \delta Z \rangle$ distribution exhibits a double-peaked structure with the first peak at ≈ 0.1, associated with the photon signal, and a second peak at ≈ 0.5, dominated by the $\pi^0 \to \gamma\gamma$ component of the background.

The number of isolated-photon events in the data is determined by a χ^2 fit to the $\langle \delta Z \rangle$ distribution in the range $0 < \langle \delta Z \rangle < 0.8$. This is illustrated in Fig. 2, and a corresponding fit was performed for each measured cross section bin, with χ^2 values of typically 1.1 per degree of freedom. In performing the fits, the relative fractions of the signal and background components were varied. Of the 18249 and 12396 events selected in the inclusive-photon and the jet samples, respectively, 8530 ± 161 and 6284 ± 132 correspond to the extracted signal.

For a given observable Y, the production cross section was determined using

$$\frac{d\sigma}{dY} = \frac{\mathcal{A}\, N(\gamma)}{\mathcal{L}\, \Delta Y}, \tag{1}$$

where $N(\gamma)$ is the number of photons extracted from the fit, ΔY is the bin width, $\mathcal{L}$ is the total integrated luminosity, and $\mathcal{A}$ is the acceptance correction and was calculated using Monte Carlo from the ratio of the number of events generated to those reconstructed in a given bin. Its value was typically around 1.2.

To evaluate the acceptances, allowance must be made for the different acceptances of the direct and the resolved processes, as modelled by PYTHIA. These components can be substantially distinguished by means of events containing a photon and a jet, in which the quantity

$$x_\gamma^{\rm meas} = \frac{E^\gamma + E^{\rm jet} - p_Z^\gamma - p_Z^{\rm jet}}{E^{\rm all} - p_Z^{\rm all}}. \tag{2}$$

is a measure of the fraction of the incoming photon energy given to the final state photon and jet, at a lowest-order approximation. The energies and longitudinal momentum components of the photon (γ), the jet and all of the EFOs are combined as indicated. Fig. 3 shows the numbers of events contributing to different bins of $x_\gamma^{\rm meas}$; a peak close to unity is seen, which can be attributed to direct events, and a tail at lower values due to resolved events. The data are compared to a 50:40 mixture of PYTHIA-simulated direct and resolved events with a 10% admixture of NLO and fragmentation events, normalised to the data. The acceptance factors were calculated using this model. Acceptance factors calculated in this way were applied both to the inclusive and to the jet data.

7 Systematic uncertainties

The most significant sources of systematic uncertainty were taken into account as follows.

- The cross sections were recalculated using HERWIG to model the signal and background events. The ensuing changes in the results correspond to an uncertainty of typically up to 8%, rising to 30% in the lower bins of $x_\gamma^{\rm meas}$.
- The energy of the photon candidate was varied by ±2%. At the same time, the energy of the jet, when measured, was varied in the same direction by an amount varying from ±4% to ±1.5% as $E_T^{\rm jet}$ varies from 4 GeV to above 10 GeV. This gave variations in the measured cross sections of typically 5-10%, or 5% for the inclusive photon measurements.
- The uncertainty in the acceptance due to the estimation of the relative fractions of direct, resolved and fragmentation events was typically ±3%.

Further systematic uncertainties were evaluated as follows:

- the dependence on the modelling of the hadronic background by the MC was investigated by varying the upper limit for the $\langle \delta Z \rangle$ fit in the range $[0.6, 1.0]$, giving variations that were typically ±2%.

The background from DIS events was found to be negligible. Other sources of systematic uncertainty were found to be negligible and were ignored; these included the modelling of the ΔR cut, the track momentum cut, the cut on $E - p_Z$, the $Z_{\rm vtx}$ cut, and the cuts on the electromagnetic fraction of the photon shower and the photon isolation. Except for the HERWIG uncertainty, the major uncertainties were treated as symmetric and added in quadrature. The common uncertainties of 1 $\rm fb^{-1}$ on the luminosity measurement and 5% on the trigger efficiency were not included in the tables and figures.

8 Results

Differential cross sections for the production of an isolated photon with and without at least one additional jet, $ep \to e'\gamma + \text{jet}$, were measured in the kinematic region defined by $Q^2 < 1$ GeV^2, $0.2 < y_{JB} < 0.7$, $-0.7 < \eta^\gamma < 0.9$, $6 < E_T^\gamma < 15$ GeV, $4 < E_T^{\text{jet}} < 35$ GeV and $-1.5 < \eta^{\text{jet}} < 1.8$ in the laboratory frame. The jets are formed according to the k_T-clustering algorithm with the R parameter set to 1.0, and photon isolation is imposed such that at least 90% of the energy of the jet-like object containing the photon belongs to the photon. If more than one jet is found within the designated η^{jet} range, that with highest E_T^{jet} is taken.

The differential cross sections as functions of x_γ^{meas}, E_T^γ, η^γ, E_T^{jet} and η^{jet} are shown in Figs. 4, 5, 6, and 7, and given in Tables TTT. The theoretical predictions described in Section 4 are compared to the measurements; theoretical uncertainties are indicated by the width of the respective shaded areas. The predictions from FGH [12] describe the shape of all the distributions reasonably well but tend to be lower than the data, especially for the inclusive cross sections. Those of BLZ [35] also describe the shape of the data reasonably well for most distributions, but the sharpness of the direct peak in the x_γ^{meas} distribution is overestimated and the jet distributions are described less well than those of the photon. For most distributions, the comparisons with theory are qualitiatively similar to those obtained by H1 in their measurements [7].

9 Conclusions

The production of inclusive isolated photons and photons with an accompanying jet has been measured in photoproduction with the ZEUS detector at HERA using an integrated luminosity of $370 \pm 7\,\text{pb}^{-1}$. The present results improve on earlier ZEUS results [2, 10] which were made with integrated luminosities of 38 and 77 pb^{-1}. Differential cross sections as functions of several variables are presented within the kinematic region defined in the laboratory frame by: $Q^2 < 1$ GeV^2, $0.2 < y_{JB} < 0.7$, $-0.7 < \eta^\gamma < 0.9$, $6 < E_T^\gamma < 15$ GeV , and, where a jet is required, $4 < E_T^{\text{jet}} < 15$ GeV and $-1.5 < \eta^{\text{jet}} < 1.8$. The order $\alpha^3\alpha_s^2$ predictions of Fontannaz *et al.* reproduce the shapes of the measured experimental distributions reasonably well, as do the predictions of Baranov *et al* in most cases.

Acknowledgements

We appreciate the contributions to the construction and maintenance of the ZEUS detector of many people who are not listed as authors. The HERA machine group and the

DESY computing staff are especially acknowledged for their success in providing excellent operation of the collider and the data-analysis environment. We thank the DESY directorate for their strong support and encouragement. We also thank M. Fontannaz, G. Heinrich and N. Zotov for providing assistance and theoretical results.

References

[1] E. Anassontzis et al., Z. Phys. C 13 (1982) 277;
WA70 Collaboration, M. Bonesini et al., Z. Phys. C 38 (1988) 371;
E706 Collaboration, G. Alverson et al., Phys. Rev. D 48 (1993) 5;
CDF Collaboration, F. Abe et al., Phys. Rev. Lett. 73 (1994) 2662;
CDF Collaboration, D. Acosta et al., Phys. Rev. Lett. 95 (2005) 022003;
DØ Collaboration, B. Abbott et al., Phys. Rev. Lett. 84 (2000) 2786;
DØ Collaboration, V.M. Abazov et al., Phys. Lett. B 639 (2006) 151.

[2] ZEUS Collaboration, J. Breitweg et al., Phys. Lett. B 413 (1997) 201.

[3] ZEUS Collaboration, J. Breitweg et al., Phys. Lett. B 472 (2000) 175.

[4] ZEUS Collaboration, S. Chekanov et al., Phys. Lett. B 511 (2001) 19.

[5] ZEUS Collaboration, S Chekanov et al., Eur. Phys. J. C 49 (2007) 511.

[6] H1 Collaboration, A. Aktas et al., Eur. Phys. J. C 38 (2004) 437.

[7] H1 Collaboration, F.D. Aaron et al., Eur. Phys. J. C 66 (2010) 17 .

[8] H1 Collaboration, F.D. Aaron et al., Eur. Phys. J. C 54 (2008) 371.

[9] ZEUS Collaboration, H. Abramowicz et al., Phys. Lett. B 715 (2012) 88.

[10] ZEUS Collaboration, S. Chekanov et al., Phys. Lett. B 595 (2004) 86.

[11] ZEUS Collaboration, S. Chekanov et al., Phys. Lett. B 687 (2010) 16.

[12] M. Fontannaz, J.Ph. Guillet and G. Heinrich, Eur. Phys. J. C 21 (2001) 303) .

[13] M. Fontannaz and G. Heinrich, Eur. Phys. J. C 34 (2004) 191) .

[14] S. Baranov, A. Lipatov and N. Zotov,, Phys. Rev. D 81 (2010) 094034.

[15] ZEUS Collaboration, U. Holm (ed.), *The ZEUS Detector*. Status Report (unpublished), DESY (1993), available on `http://www-zeus.desy.de/bluebook/bluebook.html`.

[16] N. Harnew et al., Nucl. Inst. Meth. A 279 (1989) 290;
B. Foster et al., Nucl. Phys. Proc. Suppl. B 32 (1993) 181;
B. Foster et al., Nucl. Inst. Meth. A 338 (1994) 254.

[17] A. Polini et al., Nucl. Inst. Meth. A 581 (2007) 656.

[18] M. Derrick et al., Nucl. Inst. Meth. A 309 (1991) 77;
A. Andresen et al., Nucl. Inst. Meth. A 309 (1991) 101;
A. Caldwell et al., Nucl. Inst. Meth. A 321 (1992) 356;
A. Bernstein et al., Nucl. Inst. Meth. A 336 (1993) 23.

[19] J. Andruszków et al., Preprint DESY-92-066, DESY, 1992;
ZEUS Collaboration, M. Derrick et al., Z. Phys. C 63 (1994) 391;
J. Andruszków et al., Acta Phys. Pol. B 32 (2001) 2025.

[20] M. Heilbich et al., Nucl. Inst. Meth. A 565 (2006) 572.

[21] W.H. Smith, K. Tokushuku and L.W. Wiggers, *Proc. Computing in High-Energy Physics (CHEP), Annecy, France, Sept. 1992*, C. Verkerk and W. Wojcik (eds.), p. 222. CERN, Geneva, Switzerland (1992). Also in preprint DESY 92-150B.

[22] P. Allfrey, Nucl. Inst. Meth. A 580 (2007) 1257.

[23] ZEUS Collaboration, M. Derrick et al., Phys. Lett. B 303 (1993) 183.

[24] ZEUS Collaboration, J. Breitweg et al., Eur. Phys. J. C 1 (1998) 81;
ZEUS Collaboration, J. Breitweg et al., Eur. Phys. J. C 6 (1999) 43.

[25] S. Catani et al., Nucl. Phys. B 406 (1993) 187.

[26] S.D. Ellis and D.E. Soper, Phys. Rev. D 48 (1993) 3160.

[27] J. Pumplin et al., JHEP 0207 (2002) 012.

[28] T. Sjöstrand et al., JHEP 0605 (2006) 26.

[29] K. Charchuła, G.A. Schuler and H. Spiesberger, Comp. Phys. Comm. 81 (1994) 381.

[30] A. Kwiatkowski, H. Spiesberger and H.-J. Möhring, Comp. Phys. Comm. 69 (1992) 155.

[31] L. Lönnblad, Comp. Phys. Comm. 71 (1992) 15.

[32] T. Sjöstrand, Comp. Phys. Comm. 39 (1986) 347.

[33] T. Abe, Comp. Phys. Comm. 136 (2001) 126.

[34] R. Brun et al., GEANT3, Technical Report CERN-DD/EE/84-1, CERN, 1987.

[35] N. Zotov (private communication) .

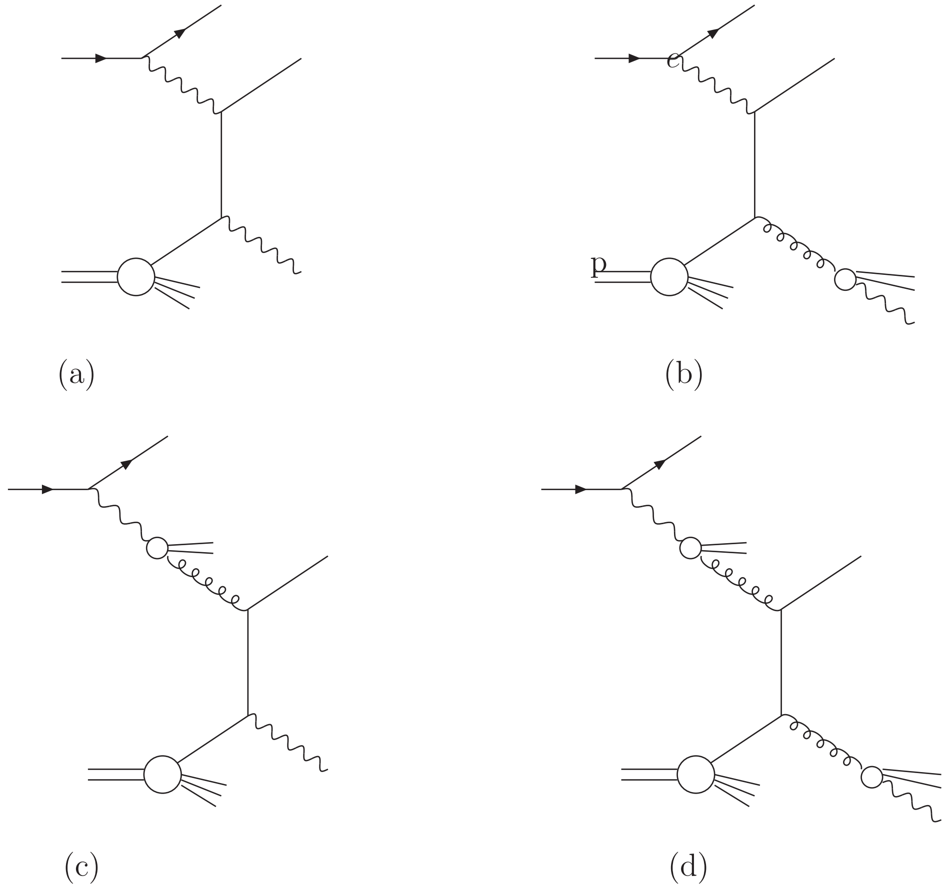

Figure 1: *Examples of direct-prompt (a), direct-fragmentation (b), resolved-prompt (c), and resolved-fragmentation (d) contributions at leading order in QCD in the photoproduction of high-energy photons.*

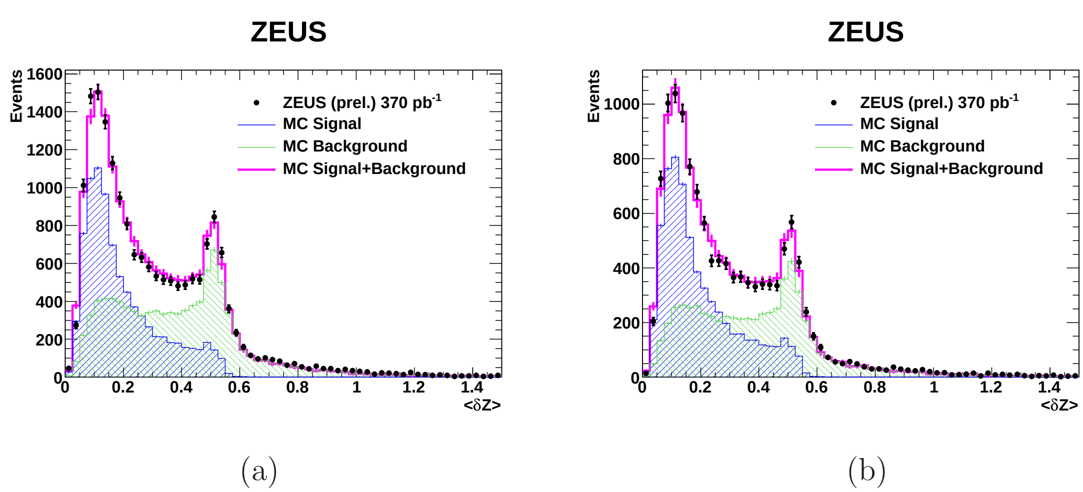

Figure 2: *Distributions of $\langle \delta Z \rangle$ for (a) inclusive photon events, (b) events with a jet, showing the fitted signal and background components.*

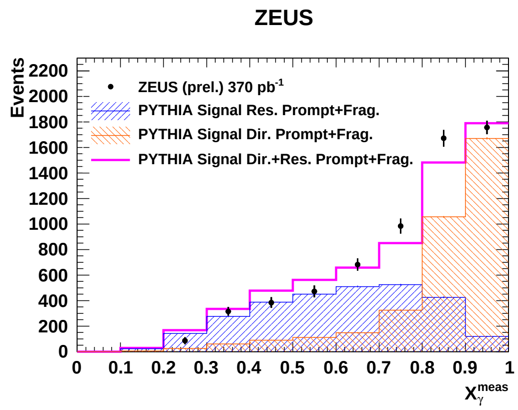

Figure 3: *Events detected for different values of x_γ^{meas}, compared to a mixture of* PYTHIA*-generated direct and resolved events, using the model described in the text. The kinematic range of the photon candidate and the jet are described in the text. The simulated events were passed through the detector simulation, but no acceptance corrections have been applied at this stage.*

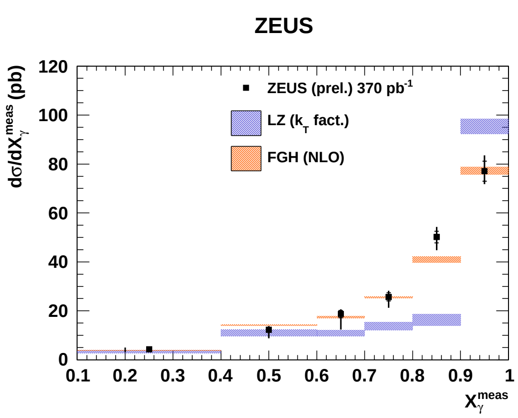

Figure 4: *Cross sections as a function of x_γ^{meas}, for events containing an isolated photon and a jet, compared to predictions from FGH and LZ. The kinematic region of the measurement is described in the text. Inner and outer vertical bars respectively denote statistical uncertainties and statistical combined with systematic.*

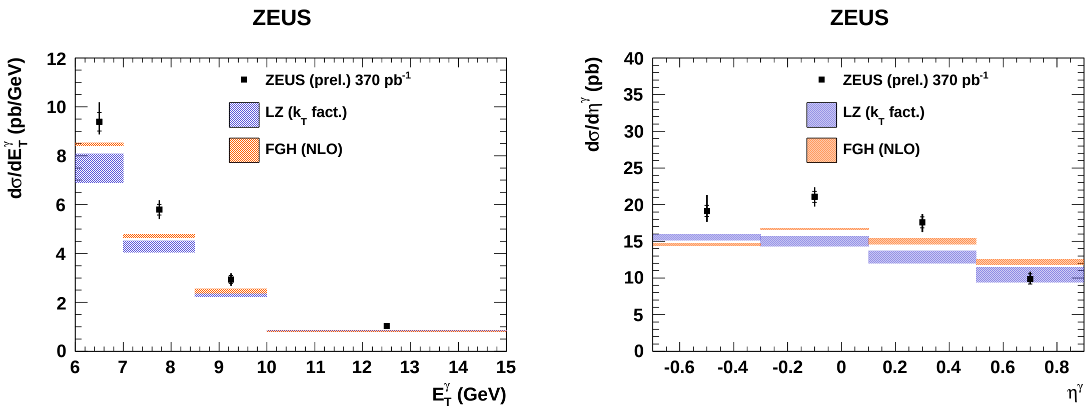

(a) (b)

Figure 5: *Cross sections as a function of (a) E_T^γ and (b) η^γ, for events containing an isolated photon compared to predictions from FGH and LZ. The kinematic region of the measurement is described in the text. Inner and outer vertical bars respectively denote statistical uncertainties and statistical combined with systematic.*

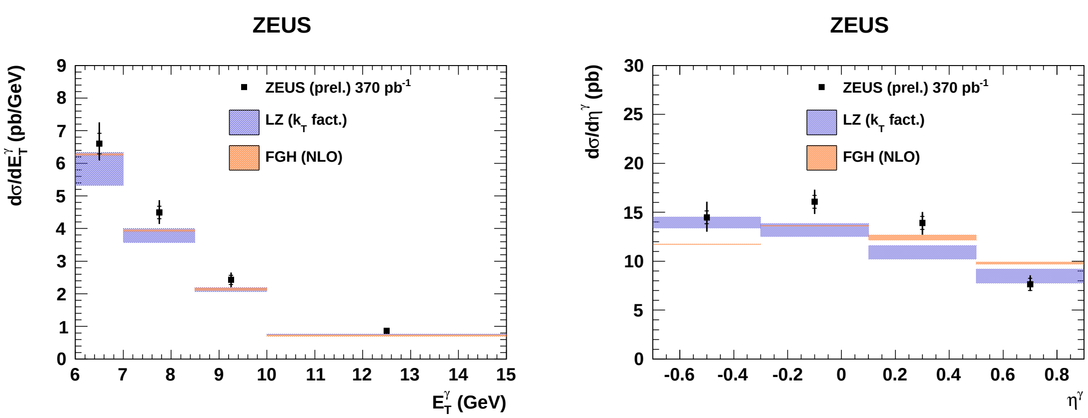

(a) (b)

Figure 6: *Cross sections as a function of (a) E_T^γ and (b) η^γ, for events containing an isolated photon accompanied by a jet (a, b) compared to predictions from FGH and LZ. The kinematic region of the measurement is described in the text. Inner and outer vertical bars respectively denote statistical uncertainties and statistical combined with systematic.*

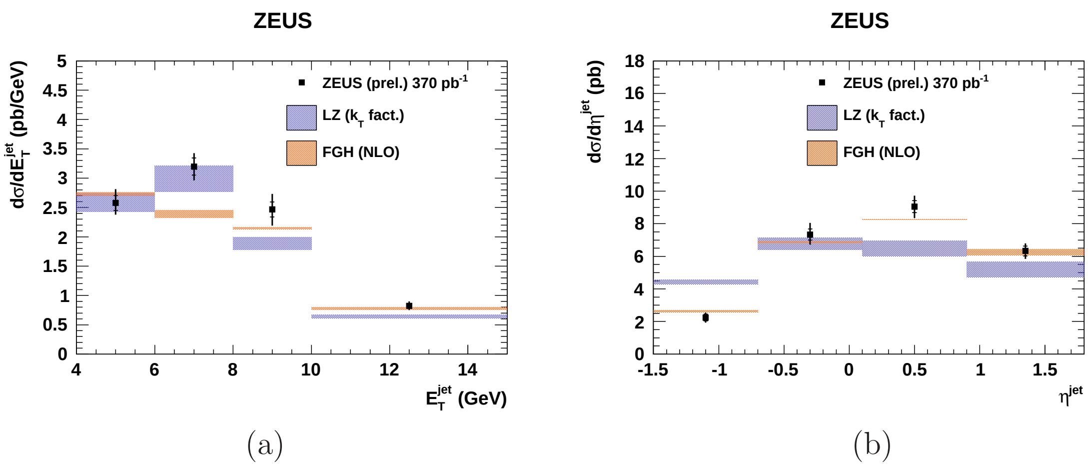

Figure 7: *Cross sections as a function of (a) E_T^{jet} and (b) η^{jet}, for events containing an isolated photon accompanied by a jet compared to predictions from FGH and LZ. The kinematic region of the measurement is described in the text.*